Int. J. Electrochem. Sci., 13 **(2018)** 7505 – 7516, doi: 10.20964/2018.08.02

International Journal of
ELECTROCHEMICAL
SCIENCE
www.electrochemsci.org

Rust Evolution and Electrochemical Properties of Field-exposed Carbon Steel in a Tropical Marine Environment

Daming Chen[1,2,*], *Xinyan Chen*[2], *Shaodong Chen*[2], *Yong Chen*[1,2]

[1] Key Laboratory of Tropical Biological Resources of Ministry of Education, Hainan University, Haikou, 570228, China
[2] College of Materials and Chemical Engineering, Hainan University, Haikou, 570228, China
[*]E-mail: daming_chen@163.com

Received: 11 November 2017 / *Accepted:* 23 March 2018 / *Published:* 5 July 2018

The corrosion behavior of carbon steel (CS) exposed in a tropical marine atmosphere for 2 years was studied by the weight loss, scanning electron microscopy (SEM), X-ray diffraction (XRD), Raman spectroscopy, and electrochemical impedance spectroscopy techniques. The results show that the corrosion layer became more loose and thick with increasing exposure time, and after 2 years exposure, the rust layer developed into the dual-layer structure. The XRD and Raman analyses confirmed that the corrosion products contained γ-FeOOH, α-FeOOH, γ-Fe_2O_3, and Fe_3O_4. The polarization curves show that the corrosion potentials (E_{corr}) and corrosion current densities (I_{corr}) changed with increasing exposure duration. Furthermore, an equivalent circuit is proposed for modeling the impedance data, and the charge transfer resistance (R_2) decreased with exposure time during 6 months and increased from 6 months to 24 months, demonstrating that the corrosion rate increased first and then decreased with exposure time.

Keywords: Carbon steel; Corrosion behavior; Rust evolution; Electrochemical properties; Tropical marine environment

1. INTRODUCTION

Metal is corroded when exposed to atmospheric environment, and atmospheric corrosion of metal is an electrochemical process, which is the sum of individual processes that take place once a thin electrolyte layer forms on the metal, resulting in the degradation of metals [1]. This corrosion behavior leads to a huge economic loss, and studies have shown that the total loss is up to 3.4% of the global economy. Hence, understanding the mechanism of atmospheric corrosion is necessary. Carbon steel (CS) is widely applied in the fields of motor vehicle, railway, and other metallic structures and equipment owing its low cost and good mechanical properties. However, most of the CS is exposed to

outdoor atmospheric environment and can be inevitably affected by different forms of atmospheric corrosion such as rural, industrial, and marine environment.

So far, many studies have been carried out to reveal the corrosion behavior of CS in different atmospheric environments by using laboratory simulation experiment. For example, Song [2] pointed out that UV illumination affects the atmospheric corrosion of Q235 CS, increasing the atmospheric corrosion and found that the rust is mainly β-FeOOH in the initial exposure stage and UV illumination accelerates the transformation of γ-FeOOH to α-FeOOH. Hideki [3] found that the spraying simulation test for the environmental factors (temperature, relative humidity, and the dew condensation) significantly affects the initial atmospheric corrosion of carbon steel. Nishimura [4] reported that the content of β-FeOOH increased with increasing concentration of Cl ions, and the resistance of rust increased with test time in a wet/dry laboratory study. Han [5] reported that the outdoor wet-dry cyclic test of CS pitting corrosion and kinetics processes follows empirical equation $D = At^n$ in the initial corrosion stage, together with a transition from corrosion acceleration to deceleration. Though laboratory simulation tests are particularly useful and not time consuming for the investigating the effect of specific environmental factors on the corrosion mechanisms and excellent results can be obtained, these accelerated corrosion tests still have problems, that is the results do not always coincide with those obtained from real atmospheric exposure test. The natural atmospheric corrosion is a complicated process, and the field-exposed condition can be affected simultaneously by many environmental factors such as temperature, humidity and Cl^- content, and SO_2 level.

In order to understand the corrosion behavior of CS in actual atmospheric conditions, some field-exposed tests have been carried out. For example, Manuel [6] figured out that chloride deposition rate plays an important role in atmospheric corrosion behavior of CS in Spain coast and found that the interior of the lamina rust comprises Fe_3O_4, while the interlaminar rust contains major α-FeOOH and β-FeOOH. Ma also found [7] that the rust composition is high effected by the amount of Cl^- deposition; β-FeOOH is produced at high Cl^-; the main rust composition is γ-FeOOH and α-FeOOH in exposure station with low or no Cl^-; and the corrosion kinetics is consistent with the equation: $C = At_1^{B_1-B_2}t^{B_2}$. Juan [8] studied the corrosion behavior of CS in Panamanian tropical atmosphere by Mössbauer spectroscopy and found that chloride content and relative humidity have a significant effect on the steel corrosion, and the main constituents are γ-FeOOH and α-FeOOH, γ-Fe_2O_3, and δ-FeOOH. Wang [9] investigated the atmospheric corrosion of CS in the Qinghai Salt Lake and found β-FeOOH, γ-FeOOH, and iowaite [$Mg_4Fe(OH)_8OCl.4H_2O$] as the main composition in the rust. Ma [10] investigated the effect of β-FeOOH on the corrosion behavior of CS in tropical marine atmospheric environment and found the outer layer with the composition of α-FeOOH, γ-FeOOH, Fe_3O_4, and an amorphous substance remained almost unchanged during the test, while the inner layer (γ-FeOOH) accelerated the corrosion process in the initial stage, and the γ-FeOOH gradually consumed and transformed to γ-Fe_2O_3, and this process was good to protect the substrate. They [11] also studied the atmospheric corrosion kinetics of CS in tropical marine environment and investigated the transition behavior in marine environments, indicating that the transition point moves forward with increasing chloride ion concentration. Although excellent results have been obtained in these studies, certain details about the corrosion mechanisms of CS in tropical marine environment still need further clarification.

Lots of cities are located in tropical marine area, and the environmental condition in this area includes high temperature, high relative humidity (RH), and high Cl^- deposition rate, as well as long duration of sunshine. CS has been used to construct basic facilities including railroad, bridges, and other outdoor equipment in this area; therefore, it inevitably encounters atmospheric corrosion. Hence, understanding the corrosion mechanism of CS in tropical marine is good for adopting appropriate corrosion protection methods and predicting the life of CS under service.

The aim of this study was to investigate the corrosion behavior of CS exposed to tropical marine atmosphere for 2 years, focusing on the corrosion kinetics, rust composition, and electrochemical properties during the field-exposed test.

2. EXPERIMENTAL

Carbon steels (Q235) were used as the test material, and the composition of Q235 is listed in Table 1. Carbon steels with the size of 100 ×100×3 mm^3 were used for the field exposed test. All the samples were ground to 1200 grit, then cleaned with acetone and ethanol, and dried before the test. After that all the samples were weighed, and the surface area was determined. All the samples facing south with an angle of 45° to the horizontal were located on Haidian island (20° 04’25” N, 110°19’47” E) with 100 meters away from the coastline, as shown in Figure 1. Five test specimens were retrieved from the test site after 3, 6, 12, and 24 months of exposure (Exposure test was carried out from 2015.8 to 2017.8). Three replicates were used to study the weight loss of samples, while the other two were used to analyze the corrosion morphology, rust composition, and electrochemical properties. The average temperature and relative humidity (RH) in Haidian island were 24 °C and 80%, respectively. In addition, the time of wetness is 2562 h/year, and Cl^- deposition rate is 110 mg/m 2 day, measured by the method described in ISO 9225.

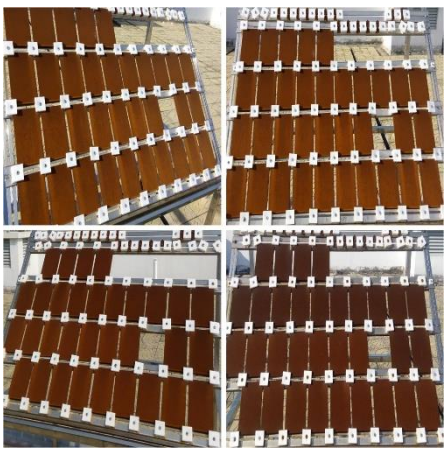

Figure 1. Exposed field of CS.

Table 1. The component of CS (wt%)

C	S	P	Mn	Si	Cu
0.176	0.023	0.019	0.057	0.233	0.033

For morphology measurement, the exposed sample was cut into piece with size 10×10×3 mm^3 and covered by an epoxy resin. Then the cross-section of the piece was polished using 1200# grade emery paper and measured by scanning electron microscopy (SEM) (Phenom proX). For rust constituents' measurement, the rust layers were scraped off using a brush and ground to powder and analyzed by Raman spectroscopy (DXRxi, Thermo Scientific) in the ranges from 50 cm^{-1} to 3000 cm^{-1}. XRD (Bruker, D2) analysis was performed using a Cu target in the 2θ range from 10° to 80° with a step width of 0.02 and a count time of 2.5 s. The electrochemical measurements were performed using Solartron (1260/1470E), and the sample was manually cut into piece with the size of 10×10×3 mm^3 and covered by an epoxy resin leaving an exposed area of 1 cm^2 as the working electrode. The measurements were carried out in 3.5 wt% NaCl solution using a conventional three-electrode cell equipped with saturated calomel electrode (SCE) as the reference electrode and platinum foil as the counter electrode. The electrochemical impedance spectroscopy (EIS) measurements were carried out in the frequency range from 100 kHz to 10 MHz at a scan rate of 0.667 mV/s with an amplitude of 10 mV, and the scan rate for polarization test is 0.1667 mV/s. Al the measurements were carried out at room temperature.

3. RESULTS AND DISCUSSION

Corrosion products of each sample were chemically removed by immersion in a specific solution (500 mL HCl + 500 mL DI water + 3.5 g HMTA) for 30 min at RT. When the corrosion products completely removed, the sample was dried at 100 °C and weighed to determine their mass loss. The weight loss was calculated using Equation (1):

$$A = (w_0 - w_1) / S \quad (1)$$

where A is the total weight loss of each sample, w_0 is the weight of the original sample, w_1 is the weight of the sample after removing the corrosion products, and S is the surface area. The average corrosion rate of CS exposed to different times was calculated as follows:

$$V_n = \frac{12(w_n - w_{n-1})}{\rho S(t_n - t_{n-1})} \quad (2)$$

where V_n is the average corrosion rate, ρ is the density of CS, t is the exposure time, n is the period of exposure (when n = 1, 2, 3, 4, indicating that CS was exposed for 3, 6, 12, and 24 months, respectively). According to Equations (1) and (2), the weight loss and the average corrosion rate can be obtained, as shown in Figure 2, indicating that there is an increasing trend in weight loss with increasing exposure time during the test. However, the average corrosion rate remarkably fluctuated during the exposure time, reached a maximum value at 6 months exposure and then decreased with increasing exposure time. Hence, it is reasonable to deduce that with increasing exposure time, the

atmospheric corrosion process would continue in tropical marine atmosphere, but the corrosion rate will decrease. Similar trend of corrosion rate for CS is reported previously [11].

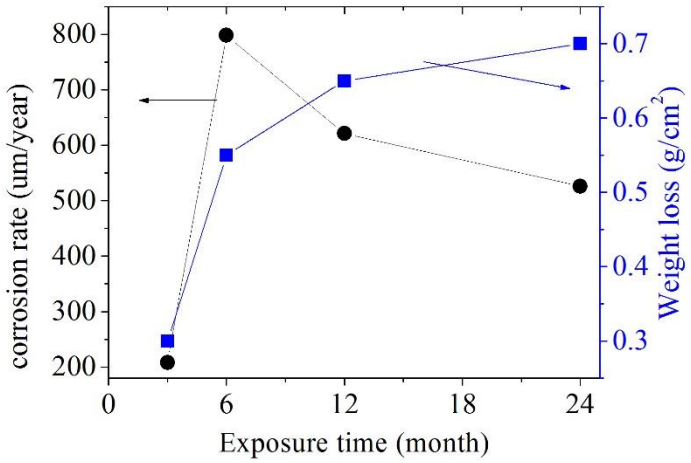

Figure 2. Weight loss and corrosion rate of CS exposed to 3 months, 6 months, 12 months, and 24 months, respectively.

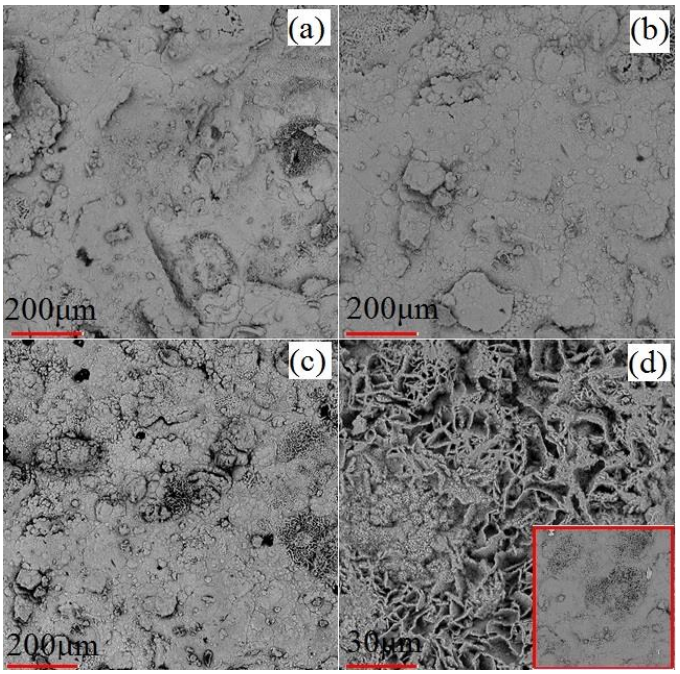

Figure 3. The morphological characteristics of rust layers with different exposure times: (a) 3 months, (b) 6 months, (c) 12 months, and (d) 24 months.

The morphological characteristics of rust layers with different exposure times are shown in Figures 1 and 3. The rust layer was yellow-orange color, when the CS was exposed to 3 months, and then gradually turned to reddish-brown with increasing exposure time to 24 months, as shown in Figur0065 1. The SEM results show that the rust layer is scale-like in the beginning and is uninterrupted and compact. With prolonged exposure time, some porous structure appears, as shown in Figure 3(b). When the specimens were further exposed to 12 months, the rust layer cracked and the

porous structure increased. As the exposure time further prolonged to 24 months, rust layer become more and more porous. This structure of rust layers can provide tunnels for the penetration of corrosive species such as water, oxygen, and chloride ions into CS substrate, further corroding the CS substrate.

The cross-sectional morphologies of the rust layers are shown in Figure 4. In the initial stage of corrosion, the rust layer is loose and thin; therefore, the corrosive species such as water, oxygen, and chloride ion can easily penetrate and attack the CS substrate, increasing the corrosion. With increasing exposure time, the rust layer becomes thicker and looser. After 24 months of exposure, the rust layer contains more and more micro-cracks and is easily scaled off. Meanwhile, the rust layer developed into dual-layer structure, and the outer layer contained γ-FeOOH, α-FeOOH, Fe_3O_4, and amorphous oxyhydroxide, while the inner layer contained γ-FeOOH, α-FeOOH, Fe_2O_3, and amorphous oxyhydroxide [10]. During the entire exposure period, the rust layer became more and more thick and loose. The tropical marine environment is proved to have lots of chloride ions, and Cl^- is the most aggressive ion among the corrosive species and penetrates easily into CS substrate to destroy the oxide layers of the rust layer [7], which is the reason of rust layer becoming thicker and looser. In contrast, once the rust layer is thick enough, it can protect the CS substrate and slow down the attack of corrosive species in marine environment [12].

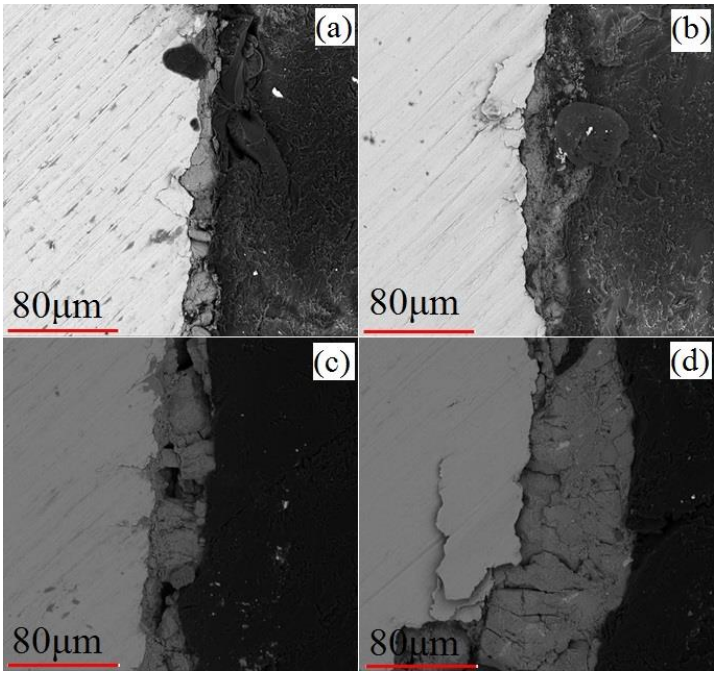

Figure 4. The cross-sectional morphologies of rust layers with different exposure times: (a) 3 months, (b) 6 months, (c) 12 months, (d) 24 months.

The X-ray diffraction (XRD) patterns of the corrosion products of CS with different exposure times are displayed in Figure 5. The result indicates that the corrosion products of CS exposed for 3 months comprised α-FeOOH, β-FeOOH, γ-FeOOH, Fe_3O_4, and γ-Fe_2O_3. With increasing exposure time to 6 months, the rust layer comprised α-FeOOH, β-FeOOH, γ-FeOOH, Fe_3O_4, and γ-Fe_2O_3, and its composition did not vary with the exposure time, even though the time prolonged to 24 months. However, α-FeOOH and γ-FeOOH were found as the primary constituents in the crystalline corrosion

products, and the intensity of α-FeOOH increased with increasing exposure duration. It is believed that the proportion of various crystalline phases among the corrosion products is closely related to the corrosion rate.

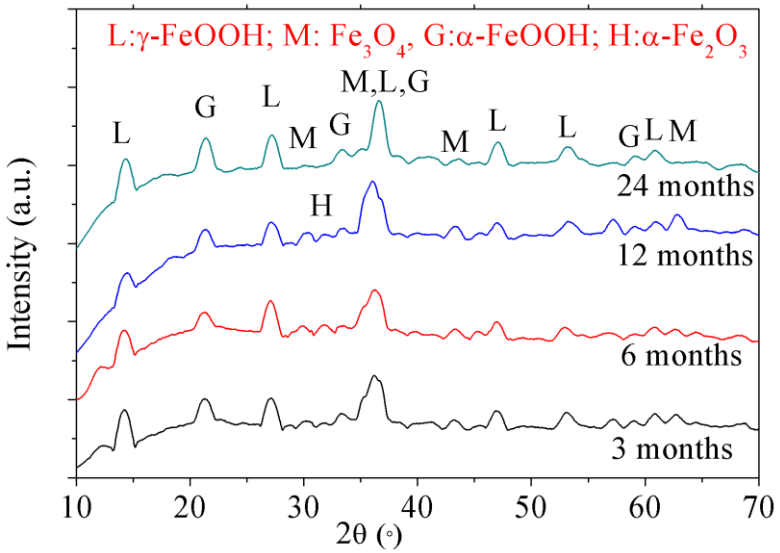

Figure 5. X-ray diffraction patterns of rust layers for CS exposed to 3 months, 6 months, 12 months, and 24 months, respectively.

Kamimura [12] proved that the mass ratio of crystalline α-FeOOH to γ-FeOOH (α/γ) can be adopted to evaluate the protective ability index of rust of CS exposed to atmospheric environments, and they found that α/γ increases with increasing exposure duration. According to the Relative Intensity Ratio method [13], the α/γ of our samples with different exposure durations can be obtained, as shown in Figure 6, indicating that α/γ increases with increasing exposure time. Ma [7] proved that γ-FeOOH phase gradually transforms to α-FeOOH in tropical marine environment, and the α-FeOOH nucleate on the surface of aggregating γ-FeOOH and gradually grow up with increasing exposure time. This trend is similar to our result.

To complement the XRD results, Raman spectroscopy was carried out to analyze the corrosion products, and the results are shown in Figure 7, indicating that 3 months exposed specimen contained several intense peaks at 216, 278, 388, 560, 670, and 1301 cm^{-1}. The peaks at 216, 278, and 1301 cm^{-1} indicate the existence of lepidocrocite (γ-FeOOH) [14]; 388 cm^{-1} is the typical peak of the Raman spectrum of goethite (α-FeOOH) [15]; the peak at 670 cm^{-1} corresponds to γ-Fe_2O_3[1]; the peak at 560 cm^{-1} belongs to magnetite (Fe_3O_4) [16]. According to the Raman analyses, the corrosion products of 3 months exposed specimen contained γ-FeOOH, α-FeOOH, γ-Fe_2O_3, and Fe_3O_4 and the corrosion products were the same when the exposure time increased. This phenomenon is in agreement with the XRD results.

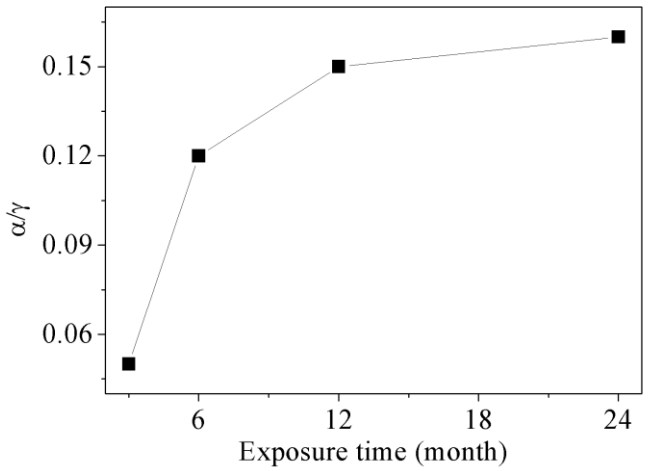

Figure 6. α/γ of rust layer for CS exposed to 3 months, 6 months, 12 months, and 24 months, respectively.

.

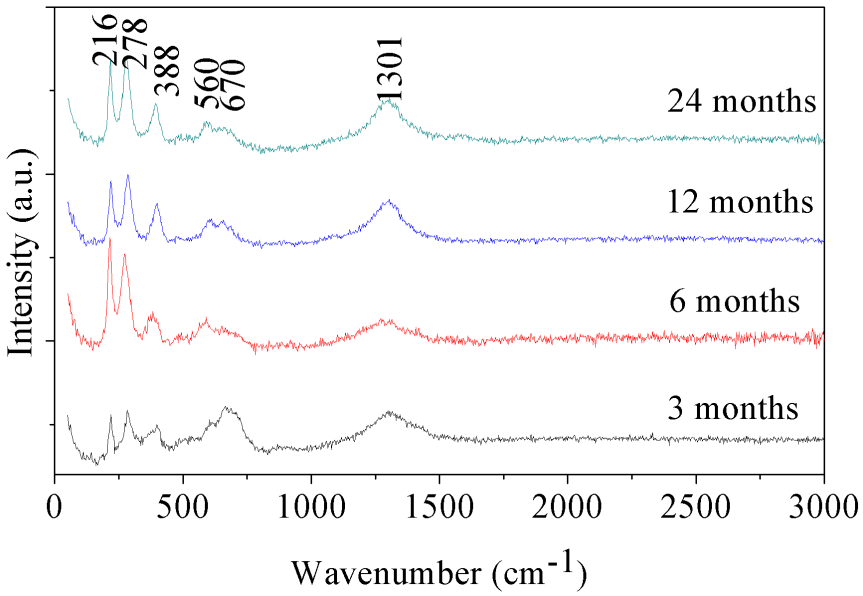

Figure 7. Raman spectrum of rust layers for CS exposed to 3 months, 6 months, 12 months, and 24 months, respectively.

The polarization curves of CS exposed to different time are shown in Figure 8, and no evident passivation behavior was observed for all the specimens. Corrosion potentials (E_{corr}) and corrosion current densities (I_{corr}) were obtained from the Tafel fitting results of the polarization curves, as listed in Table 2. The E_{corr} decreased, while the I_{corr} increased during CS exposed from 3 months to 6 months, and the E_{corr} and I_{corr} decreased after 12 months exposure. With increasing exposure time up to 24 months, the E_{corr} and I_{corr} still decreased. This tendency of I_{corr} indicates that in the initial stage of test (before 6 months), CS is less susceptible to corrosion, but after 6 months exposure, the rust layer grew

thicker, leading to the CS being less susceptible to corrosion in tropical marine environment. This behavior is in agreement with those obtained from the weight loss method.

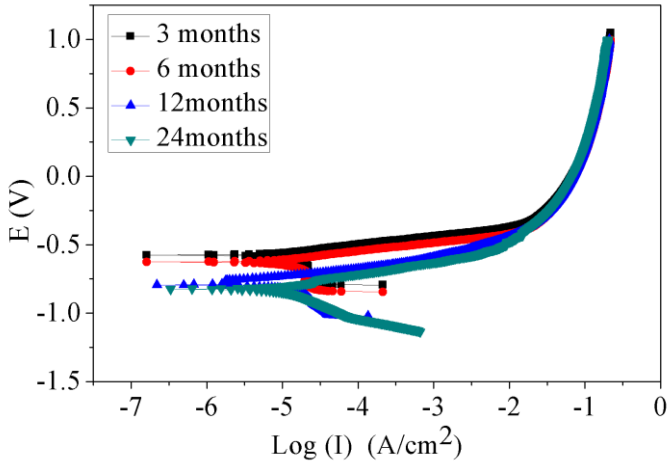

Figure 8. The polarization curves of CS exposed to 3 months, 6 months, 12 months, and 24 months, respectively.

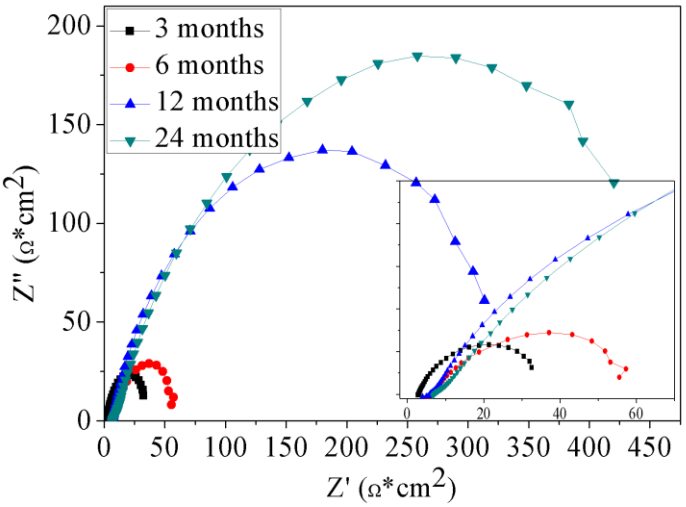

Figure 9. Nyquist spectrum of CS exposed to 3 months, 6 months, 12 months, and 24 months, respectively.

Table 2. Electrochemical parameters obtained from polarization and EIS curves.

Expoure time	3 months	6 months	12 months	24months
E_{corr} (V)	–0.53	–0.63	–0.79	–0.81
I_{corr} (μA/cm^2)	2.6	4.1	1.28	0.46
R_1 (ohm)	6.21	6.53	6.15	6.32
R_2 (ohm)	102.31	72.13	420	900.9
CPE_{dl} (μF/cm^2)	215.7	155.2	92.3	46.2

EIS was used to investigate the corrosion mechanism and evaluate the protectiveness of corrosion products layer formed on metal [17]. The Nyquist spectrum, Bode angle plots, and Bode impedance plots of CS exposed to different times are shown in Figures 9 to 11, indicating that the size of impedance semicircles increases as the exposure duration increases. All the Nyquist spectra have only one depressed capacitive loop, attributed to the dispersion effects. Such phenomenon is often ascribed to the roughness and inhomogeneities on the surface of oxide layer [18]. For the Bode impedance plots, the slope is always positive, hence, there are resistance and capacitance in the equivalent circuit, and no inductance appears. In addition, the module value and phase angle vary with the exposure time, indicating that the corrosion mechanism is different during the test. In order to obtain more information on corrosion mechanism, an equivalent circuit, as shown in Figure 12, was proposed for modeling the impedance data, and the fitting results are listed in Table 2. R_1 represents the ohmic resistance of the solution, CPE_{dl} is the double layer capacitance, and R_2 is the charge transfer resistance.

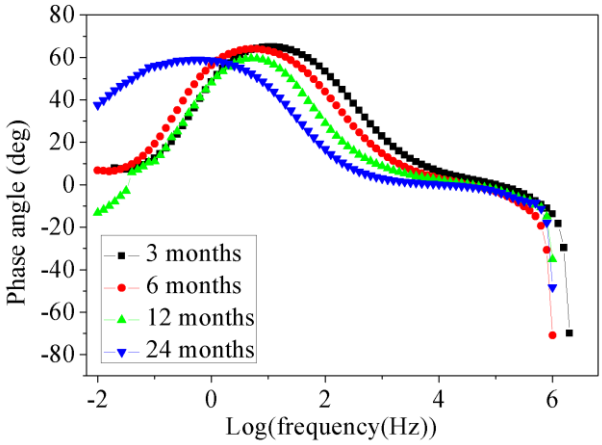

Figure 10. Bode angle plots of CS exposed to 3 months, 6 months, 12 months, and 24 months, respectively.

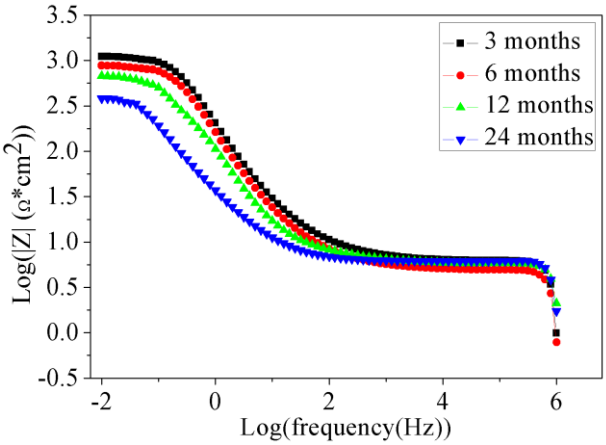

Figure 11. Bode impedance plots of CS exposed to 3 months, 6 months, 12 months, and 24 months, respectively.

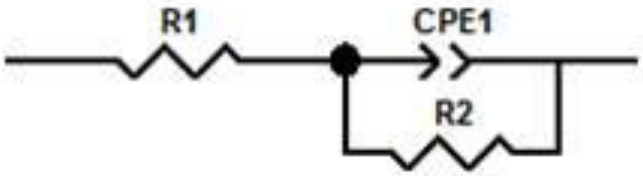

Figure 12. An equivalent circuit for CS exposed to 3 months, 6 months, 12 months, and 24 months, respectively.

R_2 is inversely proportional to the corrosion rate and was used to characterize the corrosion rate [19]. R_2 increased with exposure time during 6 months and decreased from 6 months to 24 months, demonstrating that the corrosion rate increased first and then decreased with increasing exposure time. This behavior is in agreement with the average corrosion rate measured by weight loss. Meanwhile, the CPE_{dl} decreased from that of 3 months to 12 months, and after 12 months exposure CPE_{dl} further increased. Capacitance is directly proportional to the area of the capacitor; hence various tendencies of CPE_{dl} indicate that the corrosive area of the metal/hydroxide interface to the electrolyte increased after 12 months exposure.

5. CONCLUSIONS

In this study, the corrosion behavior of the CS exposed in tropical marine environment for 2 years was investigated by weight loss, SEM, XRD, Raman, and EIS techniques. The conclusions of this study are as follow:

1) With increasing exposure time, the rust layer becomes thicker and looser, and after 24 months of exposure, it developed into dual-layer structure, and the constituent of the outer and inner layer were found to be different.

2) The XRD and Raman results confirmed that the corrosion products of 3 months exposed specimen contained γ-FeOOH, α-FeOOH, γ-Fe_2O_3, and Fe_3O_4, and were the same with increasing exposure time to 24 months.

3) The R_2 increased with exposure time during 6 months and decreased from 6 months to 24 months, demonstrating that the corrosion rate increased in the initial stage of exposure, and after 6 months exposure, corrosion rate decreased with increasing exposure time.

ACKNOWLEDGEMENTS
This study was supported by the Natural Science Foundation of Hainan Province, China (No. 20165187).

References

1. J. Alcántara, D. Fuente, B. Chico, J. Simancas, I. Díaz and M. Morcillo, *Mater.*, 10 (2017) 39.
2. L. Y. Song, Z. Y. Chen, *Corros. Sci.*, 86 (2014) 318.

3. H. Katayama, K. Noda, H. Masuda, M. Nagasawa, M. Itagaki, K. Watanabe, *Corros. Sci.* 47 (2005) 2599.
4. T. Nishimura, H. Katayama, K. Noda, T. Kodama. *Corros*., 56 (2000) 935.
5. W. Han, C. C. Yu, Z. Y. Wang, J. Wang, *Corros. Sci.*,49 (2007) 2920.
6. M. Morcillo, J. Alcantara, I. Diaz, B. Chico, J. Simancas, D. Fuente, *Rev. Metal. Madria*., 51 (2017) 2.
7. Y. T. Ma, Y. Li, F. H. Wang, *Corros. Sci*., 51 (2009) 997.
8. A. Juan, I. Josefina, *Hyperfine Interact*., 238 (2017) 37.
9. J. Wang, Z. Y. Wang, W. Ke, *Corros. Eng. Sci. Technol*., 47 (2012) 125.
10. Y. T. Ma, Y. Li, F. H. Wang, *Mater. Chem. Phys*., 112 (2008) 844.
11. Y. T. Ma, Y. Li, F. H. Wang, *Corros. Sci*., 52 (2010) 1796.
12. T. Kamimura, S. Hara, H. Miyuki, M. Yamashita, H. Uchida, *Corros. Sci*., 48 (2006) 2799.
13. C. R. Hubbard, R. L. Snyder, *Powder Diffr*. 3(1988) 74.
14. A. Demoulin, C. Trigance, D. Neff, E. Foy, P. Dillmann, V. Hostis, *Corros. Sci*., 52 (2010) 3168.
15. D. L. Faria, S. V. Silva, M. T. Oliveira, *J. Raman Spectrosc.*, 28 (1997) 873.
16. D. Neff, L. Bellot, P. Dillmann, S. Reguer, L. Legrand, *J. Raman Spectrosc*., 37 (2006) 1228.
17. Q. Cheng, S. Song, L. Song, B. Hou, *J. Electro. chem. Soc*., 160 (2013) 380.
18. Q. Cheng, Z. Chen, *Int. J. Electro. chem. Sci.*, 8 (2013) 8282.
19. Q. L. Cheng, B. Tao, L.Y. Song, W. H. Zhang, X.Y. Liu, W.H. Li, B.R. Hou, Q.Z Liu, *Corros. Sci.*,111 (2016) 61.